RSC Advances

PAPER

View Article Online
View Journal | View Issue

Cite this: *RSC Adv.*, 2021, **11**, 21813

Quick extracellular biosynthesis of low-cadmium $Zn_xCd_{1-x}S$ quantum dots with full-visible-region tuneable high fluorescence and its application potential assessment in cell imaging

Shiyue Qi,[a] Ji Chen,[a] Xianwei Bai,[b] Yahui Miao,[a] Shuhui Yang,[c] Can Qian,[a] Borong Wu,[a] Yanjun Li[a] and Baoping Xin*[a]

Received 6th June 2021
Accepted 7th June 2021

DOI: 10.1039/d1ra04371d

rsc.li/rsc-advances

The biosynthesis of metal nanoparticles/QDs has been universally recognized as environmentally sound and energy-saving, generating less pollution and having good biocompatibility, which is most needed in biological and medical fields. In the arena of chemical routes, however, biosynthesis has long been criticized for its low productivity, time-consuming process, and poor control over size, shape and crystallinity, keeping the much-needed technology away from practical application. In this work, a rapid and extracellular biosynthesis of multi-colour ternary $Zn_xCd_{1-x}S$ QDs by a mixed sulfate-reducing bacteria (SRB)-derived supernatant was carried out for the first time to solve the problems plaguing this field of biosynthesis. The results showed that about 3.5 g L^{-1} of $Zn_xCd_{1-x}S$ QDs with size of 3.50–4.64 nm were achieved within 30 minutes. The PL emission wavelength of $Zn_xCd_{1-x}S$ QDs increased from 450 to 590 nm to yield multicolor QDs by altering the molar ratio of Cd^{2+} to Zn^{2+}. The SRB-biogenic $Zn_xCd_{1-x}S$ QDs have high stability in gastric acid and at high temperature, as well as excellent biocompatibility and biosafety, successfully entering growing HeLa cells and labelling them without detectable harm to cells. The SRB-secreted peculiar extracellular proteins (EPs) play a decisive function in the time-saving, high-yield biosynthesis of PL-tuned multicolor QDs, which cover an abnormally high concentration of acidic amino acids to provide tremendous negatively charged sites for the absorption of Cd^{2+}/Zn^{2+} for rapid nucleation and biosynthesis. The strongly electrostatic connection between the QDs and the EPs and the increasing amount of EPs attached to the QDs in response to the increase of Cd^{2+} concentration account for their high stability and excellent biocompatibility.

1 Introduction

Quantum dots (QDs) are inorganic semiconductor nanocrystals with a size range of 2–10 nm. They are composed of elements such as Cd, Pb, and Hg from groups II–VI, III–IV and IV–VI of the periodic table.[1] Because the particle size of QDs is smaller than the bulk materials' Bohr radius, the energy levels pose discrete electronic energy states compared to the energy level continuum in bulk materials.[2] Owing to the quantum confinement effects and size-dependent photoemission characteristics, QDs are known for being bright, color-tunable inorganic fluorophores with narrow symmetric emission bands and high photostability.[3] Due to the unique photooptical and photovoltaic properties, QDs are broadly used in solar cells, photovoltaic devices, light-emitting diode (LED) fabrication, photodetectors and computing; particularly, they are well suited for application in the fields of biology and medicine for imaging, sensing and tracking particles or cells, including biol-abeling and biosensing, as substitutes for organic fluorophores.[2–4]

At present, wet chemical methods such as micro-emulsion, co-precipitation, sol gel, solvothermal, ultrasonic irradiation and microwave heating are the mainstream routes to commercially fabricate a variety of nanoparticles and QDs.[3,5] The chemical strategies provide excellent control over the shape and size of the nanoparticles and QDs, which is vitally important, as these parameters dominate their nanoscale properties.[6] Although the solution-based wet routes have typically governed the nanosphere, increasing concerns have arisen with regard to the negative impact on the environment owing to the use of toxic chemicals/solvents, explosive precursors, harsh reaction conditions such as extreme temperature, pressure and pH, as well as the discharge of harmful byproducts.[5,7–9] Therefore, there is an urgent need to develop green and environmentally friendly methods to synthesize nanoparticles and QDs as a viable alternative to the chemical synthesis routes.[3,5] Moreover, the chemically manufactured nanoparticles and QDs

[a]*School of Materials Science and Engineering, Beijing Institute of Technology, Beijing 100081, P. R. China*

[b]*Shenzhen Institutes of Advanced Technology, Chinese Academy of Sciences, Shenzhen 518055, P. R. China*

[c]*Everdisplay Optronics (Shanghai) Co., Ltd., Shanghai 201506, P. R. China*

are usually inadequate for biological and medical systems due to poor biocompatibility.[10,11]

Biological synthesis follows the green chemistry principle, which is more acceptable in terms of environment friendliness, energy savings, the use of ambient temperatures and pressures, the use of renewable materials as electron donors, and the production of biocompatible matter.[3,10] A wide range of metal nanoparticles and QDs have therefore been synthesized by diverse microorganisms and biomolecules in the past 20 years.[5,12] However, microbial biosynthesis of metal nanoparticles and QDs suffers from some disadvantages, which severely block its commercial application. The main shortcoming is poor control of size, morphology, structure, property, and crystallinity, along with difficult separation of the products from microbes. Another major drawback is the slow production rate compared to chemical synthesis routes, making the biological production process more time consuming.[3,13] Nevertheless, in recent years, these problems have gradually been solved through developing extracellular biosynthesis processes, employing sulfate-reducing bacteria (SRB), changing incubation time and altering metal concentration to ease the separation process, increase the production efficiency, adjust the fluorescence spectra and control the size of nanoparticles, respectively.[14–17]

Among various semiconductor metal nanomaterials, the biosynthesis of metal sulfides has long been the most appealing research topic because of the abundant sulfur on Earth as well as the unique optical and electronic properties and wide applications of metal sulfides.[3,10,18,19] In particular, the bio-manufacture of ZnS and CdS QDs has drawn considerable attention for applications in the fields of biology and medicine for imaging, sensing, tracking and drug delivery, owing to their high optical efficiency, high fluorescence intensity and low cost.[3,10,12] ZnS is a wide-bandgap photoluminescent material with low toxicity and high photocorrosion resistance, but it has poor absorption over the visible light range,[20] while CdS has a narrow bandgap with strong absorption in the visible light range, but it is highly toxic and has poor photocorrosion resistance.[21,22] For zincblende ZnS and CdS, their lattice constants under ambient temperature are, respectively, 5.406 Å and 5.835 Å. Such a low lattice mismatch indicates that introducing Zn into the CdS lattice to form $Zn_xCd_{1-x}S$ alloyed QDs may be a practical way to engineer emitters with both high bandgap emission efficiency and reduced toxicity,[23–25] thus covering the shortage of single ZnS and CdS.[26]

As a ternary semiconductor, $Zn_xCd_{1-x}S$ alloyed QDs possess a continuous, adjustable bandgap, high carrier mobility and high quantum yield,[27] thus displaying wider potential applications than the discrete-bandgap binary materials ZnS and CdS QDs in phosphorescent differential sensing,[28] biological markers,[29] glucose sensing[30] and immunosorbent assay.[31] Especially, $Zn_xCd_{1-x}S$ alloyed QDs open up a great possibility for *in vitro* and *in vivo* imaging, labeling and sensing in medicine and life science due to their tunable fluorescence characteristics.[32] For more competent $Zn_xCd_{1-x}S$ QDs in the fields of biology and medicine, the mainstream chemical synthesis methods have been concentrating on both tunable fluorescence and toxicity reduction.[33–35] Tunable fluorescence is attained by increasing the cadmium content to realize fluorescence red-shift and form multicolor QDs, while toxicity reduction is achieved through the formation of a passivation layer on the surface of $Zn_xCd_{1-x}S$ QDs using highly biocompatible molecules.[36] However, the elevated Cd content inevitably leads to increased toxicity of the $Zn_xCd_{1-x}S$ QDs,[35] while the formation of a passivation layer using expensive biocompatible molecules increases production cost.[34] Low-cost synthesis of Zn_x-$Cd_{1-x}S$ alloyed QDs with low Cd content and red shift to full-visible-region tunable high fluorescence is of importance for applications in medicine and life sciences.

A great number of studies have focused on the biosynthesis of metal sulfides ZnS and CdS QDs as binary semiconductors, but no biosynthesis of ternary semiconductor $Zn_xCd_{1-x}S$ alloyed QDs has been available, to date. In previous work, the highest ZnS QD extracellular biosynthesis rate of 35.0–45.0 g per L per month was obtained by mixed sulfate-reducing bacteria (SRB), which secreted peculiar extracellular proteins (EPs) containing extraordinary amino acids to strongly mediate the biosynthesis of binary metal sulfide QDs.[15] In the current work, the mixed SRB was utilized for extracellular biosynthesis of low-toxicity and adjustable-fluorescence ternary semiconductor $Zn_xCd_{1-x}S$ alloyed QDs for the first time. The $Zn_xCd_{1-x}S$ QDs, with low Cd content, from 0.2 to 0.02 in molar ratio of Cd/Zn, and a tunable fluorescence from 450 nm to 590 nm, were biosynthesized at a high yield, and the high biocompatibility, high stability and low toxicity of the resulting $Zn_xCd_{1-x}S$ QDs were assessed completely.

2 Results and discussion

2.1 Biosynthesis of $Zn_xCd_{1-x}S$ QDs with full-visible-region tunable PL

2.1.1 Phase analysis of the resulting products by XRD and EDX. The XRD images displayed three major characteristic diffraction peaks (111), (220) and (311) in the as-prepared products from $Zn^{2+}/Cd^{2+} = 0:1$ and $Zn^{2+}/Cd^{2+} = 1:0$, which are well indexed to the cubic sphalerite structure of CdS (JCPDS Card No. 65-2887) and ZnS (JCPDS Card No. 65-5476), respectively (Fig. 1). This showed the SRB-derived supernatant is

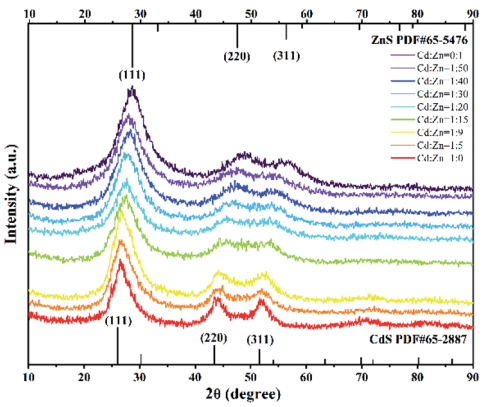

Fig. 1 XRD patterns of the resulting products biosynthesized by the SRB-derived supernatant at different molar ratios of Cd^{2+} and Zn^{2+} ranging from 1 : 50 to 1 : 5. The ratio of Cd^{2+}/Zn^{2+} at 1 : 0 and Cd^{2+}/Zn^{2+} at 0 : 1 served as controls for CdS and ZnS, respectively. The two sets of lines on the *X*-axis (JCPDS No. 65-5476 and JCPDS No. 65-2887) are the standard spectra for ZnS and CdS.

capable of biosynthesizing both CdS and ZnS as controls. The resulting products from different molar ratios of Cd^{2+} to Zn^{2+} of 1 : 50 to 1 : 5 also showed three major characteristic diffraction peaks, respectively symbolizing lattice planes (111), (220) and (311), indicating a quick synthesis of ternary $Zn_xCd_{1-x}S$ by the SRB-derived supernatant. Compared to the hollow ZnS and CdS, the XRD peak position of the (111) plane of $Zn_{1-x}Cd_xS$ was slightly shifted to lower diffraction angles (2θ) from 29.2 to 28.6, 28.5, 28.3, 28.1, 27.8, 27.4, 26.8 and 26.6, respectively, as the concentrations of Cd gradually increased (Fig. 1). No impurity peaks occurred in the XRD patterns of $Zn_{1-x}Cd_xS$, displaying the high purity of the biosynthesized $Zn_{1-x}Cd_xS$ crystals. The XRD characteristics of $ZnxCd_{1-x}S$ obtained in this study are completely consistent with those obtained in previous literature.[24,35] The EDX images further revealed that the actual molar ratios of Zn^{2+} to Cd^{2+} in the biosynthesized $Zn_{1-x}Cd_xS$ were very close to that in the mixed solutions of Zn^{2+} and Cd^{2+}, and that total molar concentrations of Zn^{2+} and Cd^{2+} were almost equal to that of the sulfur moiety (S^{2-}), accounting for the high purity of the crystal materials (Fig. 2). Elements C, O and P were detected because of the existence of EPs, which adhered to the as-prepared products.[15] As a result, the structural similarity between ZnS and CdS and relatively small discrepancy in their bond lengths facilitate the biosynthesis of $Zn_xCd_{1-x}S$.[37]

2.1.2 Shape and size of the as-prepared $Zn_xCd_{1-x}S$ by TEM and HRTEM. The biosynthesized ternary $Zn_xCd_{1-x}S$ QDs were analyzed using TEM/HRTEM to accurately understand their structure, morphology and size. The TEM photographs reveal that all the as-prepared $Zn_xCd_{1-x}S$ products with different molar ratios of Zn^{2+} to Cd^{2+} were monodisperse, well distributed, fairly uniform spheres (Fig. 3a–i). The average crystallite size (ACS) of the as-prepared $Zn_xCd_{1-x}S$ is 3.50–4.64 nm (Fig. 3a1–3i1), suggesting that the SRB-derived supernatant rapidly fabricated $Zn_xCd_{1-x}S$ QDs, independent of the molar ratio of Cd^{2+} to Zn^{2+}. The HRTEM images depict clear lattice fringes of the nanocrystalline $Zn_xCd_{1-x}S$ QDs' cubic structure (Fig. 3a2–3i2), exhibiting that the $Zn_xCd_{1-x}S$ QDs have good crystallinity. The measured interplanar distance d_{hkl} values of alloyed $Zn_xCd_{1-x}S$ QDs ($0 < x < 1$) are smaller than the corresponding standard values $d_{(111)} = 3.36$ Å of CdS (JCPDS: 65-2887) and larger than $d_{(111)} = 3.12$ Å of ZnS (JCPDS: 65-5476) cubic structures; this was due to the substitution of Cd^{2+}, with a greater ionic radii of 0.95 Å, by the smaller Zn^{2+}, with an ionic radii of 0.74 Å, in the lattice sites of CdS nanocrystals.[35] Based on the same reason, the lattice parameter a from HRTEM pictures also became less with the decrease of molar ratio of Cd^{2+} to Zn^{2+} in the $Zn_xCd_{1-x}S$ QDs, which is consistent with those deduced from XRD images (Table 1).

The crystalline interplanar spacing in the HRTEM images also proved that the synthesized products were pure ternary $Zn_xCd_{1-x}S$ QDs rather than mixtures of ZnS and CdS. If a mixture of ZnS and CdS exists, the crystalline interplanar spacing would be either ZnS or CdS. However, the crystalline interplanar spacing of the prepared product, as pure ternary $Zn_xCd_{1-x}S$ QDs, lies between ZnS and CdS. In this study, the measured interplanar distance values (d_{hkl}) of alloyed $Zn_xCd_{1-x}S$ QDs ($0 < x < 1$) are smaller than

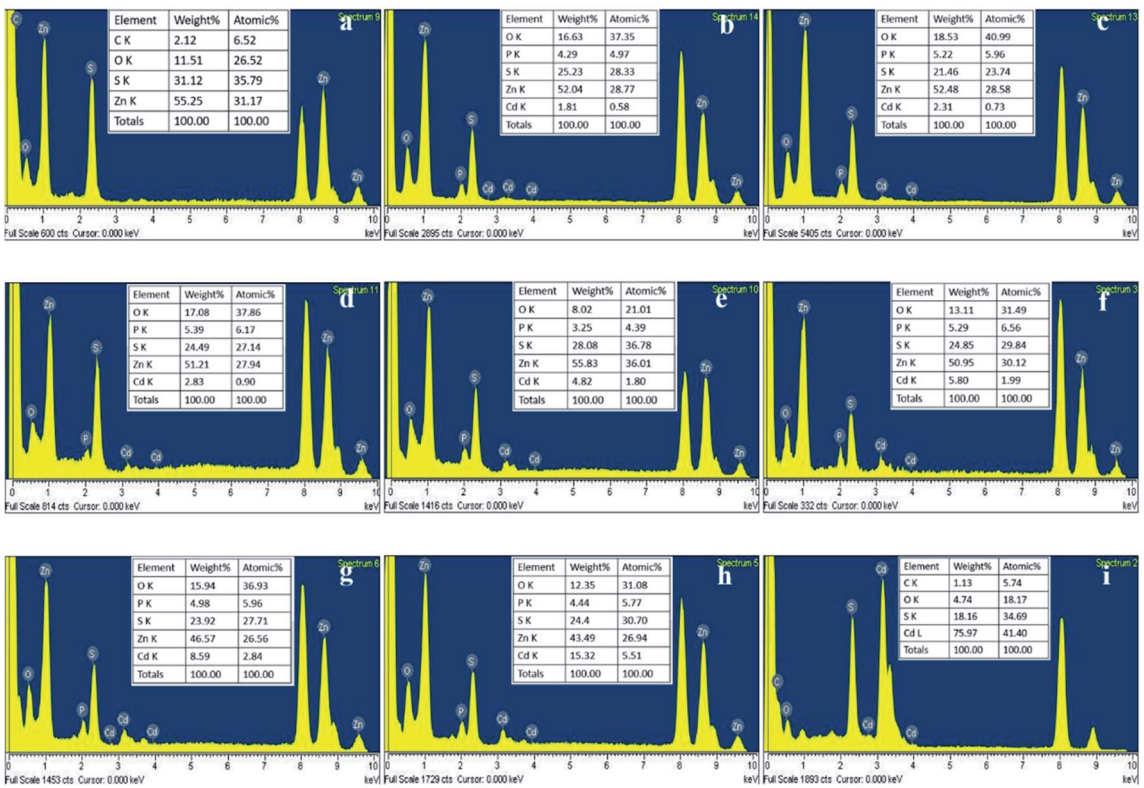

Fig. 2 EDS patterns of the as-prepared $Zn_xCd_{1-x}S$ with different molar ratios of Cd/Zn. The molar ratios of Cd/Zn = 0 : 1 (a), 1 : 50 (b), 1 : 40 (c), 1 : 30 (d), 1 : 20 (e), 1 : 15 (f), 1 : 9 (g), 1 : 5 (h), 1 : 0 (i). The appearance of copper peaks is due to the grid for TEM analysis.

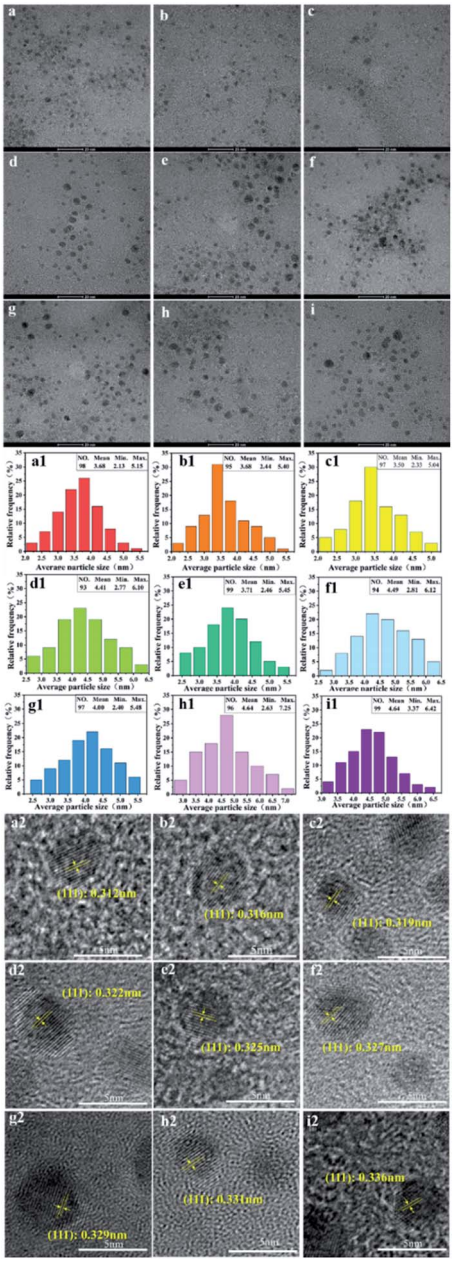

Fig. 3 TEM, HRTEM and size distribution of the SRB-derived ternary $Zn_xCd_{1-x}S$ alloyed QDs at different molar ratios of Cd/Zn. TEM of Cd/Zn = 0 : 1 (a), 1 : 50 (b), 1 : 40 (c), 1 : 30 (d), 1 : 20 (e), 1 : 15 (f), 1 : 9 (g), 1 : 5 (h), 1 : 0 (i); the particle size distribution of Cd/Zn = 0 : 1 (a1), 1 : 50 (b1), 1 : 40 (c1), 1 : 30 (d1), 1 : 20 (e1), 1 : 15 (f1), 1 : 9 (g1), 1 : 5 (h1), 1 : 0 (i1); HRTEM images of Cd/Zn = 0 : 1 (a2), 1 : 50 (b2), 1 : 40 (c2), 1 : 30 (d2), 1 : 20 (e2), 1 : 15 (f2), 1 : 9 (g2), 1 : 5 (h2), 1 : 0 (i2).

the corresponding standard values $d_{(111)} = 3.36$ Å of CdS (JCPDS: 65-2887) and larger than $d_{(111)} = 3.12$ Å of ZnS (JCPDS: 65-5476) cubic structures. Based on the above analysis, the product by prepared biological means is purely alloyed $Zn_xCd_{1-x}S$ QDs rather than a mixture of ZnS and CdS.

2.1.3 PL of the biosynthesized ternary $Zn_xCd_{1-x}S$ alloyed QDs. A strong PL is necessary for the applications of QDs in biolabeling and biosensing in life science and medicine. Especially, multicolor QDs are highly desired because they can be

Table 1 Lattice parameters of cubic $Zn_xCd_{1-x}S$ alloyed nanoparticles

	Interplanar distance $d_{(111)}$ (Å)		Lattice constant (a)	
Cd/Zn	XRD	HRTEM	XRD	HRTEM
0 : 1	3.06	3.12	5.30	5.40
1 : 50	3.12	3.16	5.40	5.47
1 : 40	3.13	3.19	5.42	5.53
1 : 30	3.15	3.22	5.46	5.58
1 : 20	3.17	3.25	5.49	5.63
1 : 15	3.21	3.27	5.56	5.66
1 : 9	3.25	3.29	5.63	5.70
1 : 5	3.33	3.31	5.77	5.73
1 : 0	3.35	3.36	5.80	5.82

applied for the simultaneous biolabeling and biosensing of multiple target cells and biomolecules.[2] Therefore, the PL of the SRB-derived $Zn_xCd_{1-x}S$ QDs and the variation of PL curves under various molar ratios of Cd^{2+} to Zn^{2+} were characterized (Fig. 4). It was observed that the SRB-derived $Zn_xCd_{1-x}S$ QDs displayed rather strong PL activity and that PL emission shifted from 450 nm to 590 nm, which almost covers the entire visible spectral region, when the molar ratio of Cd^{2+} to Zn^{2+} increased from 1 : 50 to 1 : 5, indicating that the absorption and emission peaks of the SRB-synthesized $Zn_xCd_{1-x}S$ QDs can be easily tuned by simply changing the ratio of precursor heavy metals in the solution. As an excellent blue emitter, the PL peak of $Zn_xCd_{1-x}S$ QDs was redshifted with difficulty to 460–596 nm when the ratio of Cd/Zn in synthesized QDs was increased to 0.25–1.0, and even as high as 4–9, using wet chemical methods.[24,33–35] In contrast, the current study demonstrates that the SRB biosynthesis not only carried out quick and controlled production of $Zn_xCd_{1-x}S$ QDs with tunable PL but also easily allowed redshift to 450–590 nm at a very low Cd/Zn ratio of 0.02–0.2.

2.1.4 Productivity of the $Zn_xCd_{1-x}S$ alloyed QDs with tunable PL. For a long time, the low production rate of QDs has been criticized as a major drawback of biosynthesis compared to wet chemical synthesis.[3] Therefore, improving the

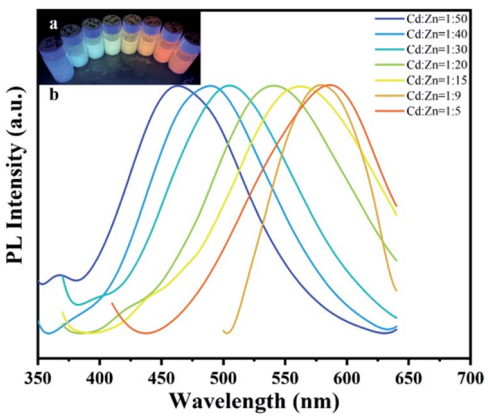

Fig. 4 PL spectra of the SRB-derived ternary $Zn_xCd_{1-x}S$ alloyed QDs at different molar ratios of Cd/Zn. The molar ratios of Cd^{2+} and Zn^{2+} ranged from 1 : 50 to 1 : 5. Inset: image of the QDs under 350 nm UV radiation.

Table 2 Productivity of SRB-synthesized $Zn_xCd_{1-x}S$ alloyed QDs

Molar ratio of Cd/Zn	Yield (g L^{-1})	Utilization rate of metal (%)
1 : 5	3.70	43.1
1 : 9	3.59	44.3
1 : 15	3.53	42.9
1 : 20	3.50	42.5
1 : 30	3.48	44.3
1 : 40	3.46	43.7
1 : 50	3.46	43.9

production rate of QDs is an urgent issue for the practical application of biosynthesis.[10] The unique SRB is likely to thoroughly solve the problem in the biosynthesis of metal sulfide QDs, which yielded the highest-ever ZnS QDs biosynthesis rate of 35.0–45.0 g per L per month (2.91–6.79 g L^{-1} by 2–6 days' growth in SRB), dominated by a peculiar EP with an abnormally high concentration of acidic amino acids.[15] However, the PL of binary metal sulfide QDs could not be controlled by altering the growth stage of SRB for the high-productivity biosynthesis of multicolor QDs. In this study, the unique SRB was first applied to manufacture ternary $Zn_xCd_{1-x}S$ QDs for the purpose of biosynthesizing multicolor QDs by simply regulating the molar ratio of Zn^{2+} and Cd^{2+} as precursors. It was shown that the quick *in vitro* biosynthesis by SRB-generated supernatant yielded PL-tuned $Zn_xCd_{1-x}S$ QDs with rather high productivity efficiency of approximately 3.5 g L^{-1} independent of the molar radio of Cd/Zn, with an average metal utilization rate of 43.5% (Table 2). The biosynthesized productivity rate of PL-tuned $Zn_xCd_{1-x}S$ QDs is almost comparable to that obtained by wet chemical synthesis.[24]

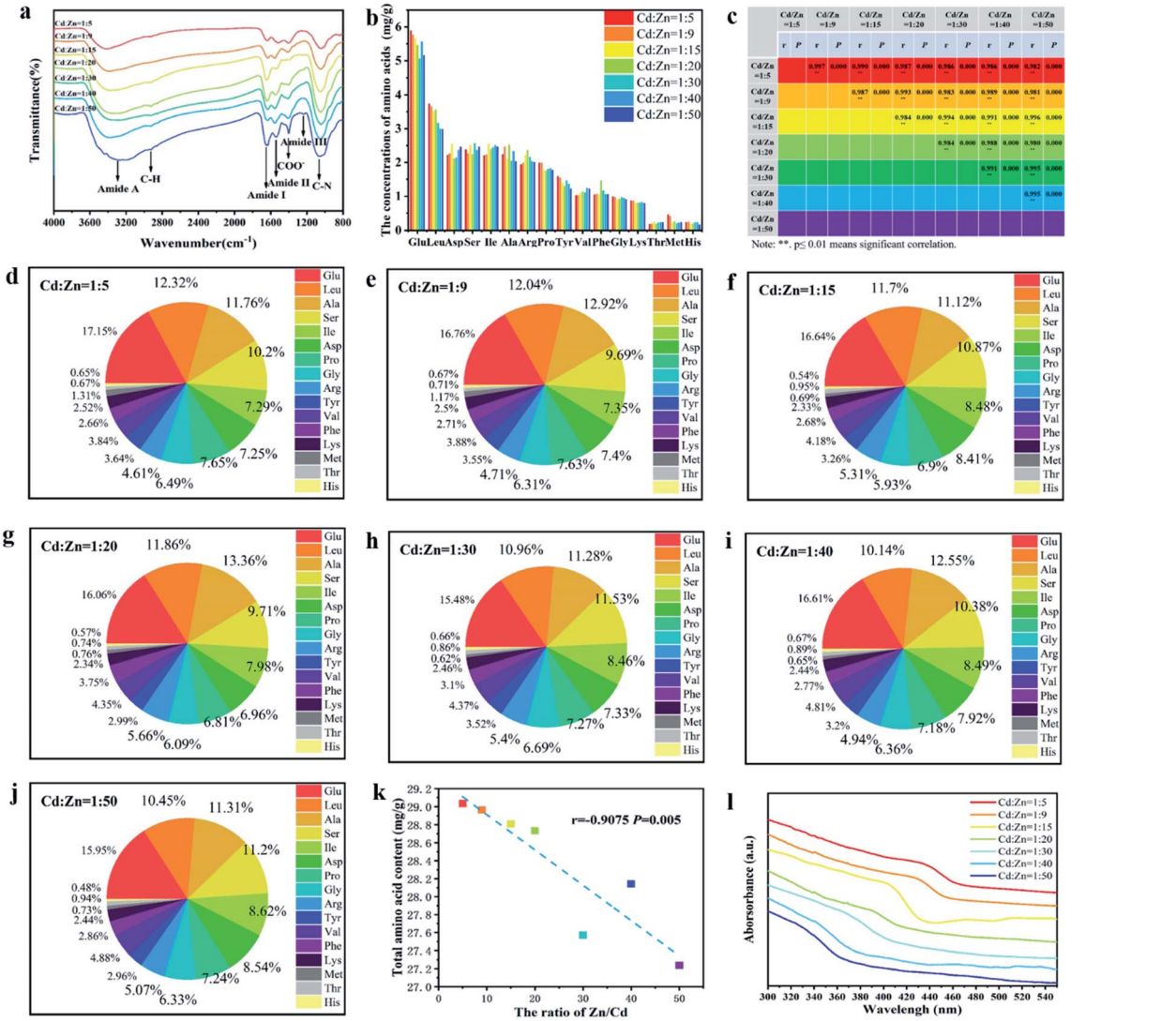

Fig. 5 FTIR and UV-vis images of the SRB-derived $Zn_xCd_{1-x}S$ QDs as well as the contents of adhered EPs and their amino acid compositions under different molar ratios of Cd/Zn. FTIR spectrum of the $Zn_xCd_{1-x}S$ QDs (a), the amino acid species of the adhered EPs and their contents (mg g^{-1}) in the as-prepared $Zn_xCd_{1-x}S$ QDs (b), similarity analysis of amino acid composition and percentage contents (c), percentage of each amino acid under different molar ratios of Cd/Zn ranging from 1/5 to 1/50 (d–j), Pearson correlation analysis between the ratio of Zn/Cd and total amino acid content (k), UV-vis absorption of the SRB-derived $Zn_xCd_{1-x}S$ alloyed QDs at different molar ratios of Cd^{2+} and Zn^{2+} from 1 : 5 to 1 : 50 (l).

2.2 EP's role in mediating $Zn_xCd_{1-x}S$ QD synthesis and enhancing PL redshift

The functional groups on the surface of $Zn_xCd_{1-x}S$ QDs were analyzed using FTIR to explore the interactions between the $Zn_xCd_{1-x}S$ QDs and SRB-derived biomolecules during biosynthesis (Fig. 5a). It was confirmed that the SRB-derived $Zn_xCd_{1-x}S$ QDs contained abundant functional groups, pointing to the amide (3293 cm^{-1}, 1651 cm^{-1}, 1541 cm^{-1}, 1240 cm^{-1} and 1057 cm^{-1}), C–H (2927 cm^{-1}) and COOH (1405 cm^{-1}) as distinct signals of protein functional groups,[15,38] suggesting that the quick *in vitro* synthesis of $Zn_xCd_{1-x}S$ QDs is mediated by EPs. A further analysis was carried out to explore the species and amino acid contents of the QD-adhered EPs at different molar ratios of Cd^{2+}/Zn^{2+} (Fig. 5b). It was found that the biosynthesized $Zn_xCd_{1-x}S$ QDs from different molar ratios of Cd^{2+}/Zn^{2+} have almost identical amino acid compositions and percentage contents (Fig. 5c), demonstrating that the quick *in vitro* biosynthesis of $Zn_xCd_{1-x}S$ QDs under different molar ratios of Cd^{2+}/Zn^{2+} is mediated by the same EPs (Fig. 5d–j). The mediated EPs include high total concentrations of acidic amino acids (22.8–25.0 mol%) and extremely high total concentrations of nonpolar amino acids (51.7–55.0%), with Glu and Leu, respectively, ranking first (15.5–17.2%) and second (10.1–12.3%) as acidic and nonpolar amino acids. The high content of negatively charged acidic amino acids offers a very large number of sites for absorption of Zn^{2+} and Cd^{2+} by the EPs to induce massive nucleation, as the first step for the quick biosynthesis of $Zn_xCd_{1-x}S$ QDs. On the other hand, the extremely high nonpolar amino acid content causes a strong hydrophobic bridging and interlinkage of the EPs to form smaller cavities that control the growth of $Zn_xCd_{1-x}S$ QDs.[15]

More interestingly, it was a surprise to discover that the amount of EPs adhered to $Zn_xCd_{1-x}S$ QDs was significantly elevated with the increase of Cd^{2+} concentration (a highly toxic metal) in the ternary alloyed QDs (Fig. 5k). This phenomenon might be due to a unique detoxification mechanism by the peculiar SRB through coating by the EPs free from cysteine to decrease the toxicity of toxic heavy metals,[15] different from the most common detoxification mechanisms by phytochelatin (PC) and metallothionein (MT), which are rich in cysteine, to chelate heavy metal ions *via* the thiol groups.[39,40] Because the SRB can produce a large quantity of H_2S (S^{2-}) at a high speed due to its dissimilatory nature, it secretes the unique cysteine-free EPs containing high acidic amino acid content to strongly absorb the toxic metals by electrostatic attraction as an efficient detoxification method. In contrast, the detoxification mechanisms guided by PC and MT to chelate heavy metal ions using cysteine is inefficient when facing a high content of toxic heavy metals. The efficient detoxification mechanism by the unique EPs may be linked to a smart strategy of SRB to deal with high concentrations of toxic metals.

The adhered EPs contain various amino acids, including acidic and nonpolar amino acids. The short chains (C–H, N–H, O–H) of the amino acid or the swing of the unbonded dangling bonds (C–C, C–N) result in energy loss of the nanocrystal charge radiation transition in the form of phonons (heat energy), causing redshift in the luminescence peaks.[35] Because more EPs were adhered to the $Zn_xCd_{1-x}S$ QDs in the case of high Cd^{2+} concentration, a greater electron transition energy loss occurred due to the increased amino acid content, leading to a larger redshift in the UV-vis absorption from 340 to 440 nm when the molar ratio of Cd^{2+}/Zn^{2+} gradually rose from 1/50 to 1/5 (Fig. 5l). Accordingly, an increasing redshift of PL spectra occurred from 450 to 590 nm at a very low Cd/Zn ratio of 0.2–0.02 because of the enhancing effect of the increasing EP coating on the $Zn_xCd_{1-x}S$ QDs (Fig. 4). Both the low Cd^{2+} concentration and high EP content bring about low biotoxicity of the ternary QDs with tunable multicolour, covering almost the whole visible region, which is of importance for their wide application in the fields of life science and medicine.[32]

2.3 Gastric acid and thermal stability of biosynthesized $Zn_xCd_{1-x}S$ QDs

The stability of structure and fluorescence is necessary for the practical application of the ternary $Zn_xCd_{1-x}S$ QDs in biolabeling and biosensing for imaging, tracking and sensing particles or cells.[2–4] Hence, the changes in XRD and PL of the biosynthesized $Zn_xCd_{1-x}S$ QDs with the molar ratio of Cd^{2+}/Zn^{2+} at 1 : 30 in simulated gastric acid or at higher temperature were monitored (Fig. 6). The results showed that the XRD image of $Zn_xCd_{1-x}S$ QDs almost remained unchanged in the simulated gastric acid for 3 days or after heat treatment at as high as 150 °C for 2 h (Fig. 6a and b), indicating that the biosynthesized $Zn_xCd_{1-x}S$ QDs have a highly stable chemical structure and are resistant to both gastric acid and high temperature. However, a slight decrease occurred in the PL intensity in both cases, with 87% and 80% of PL intensity retention at the maximum emission peak in the simulated gastric acid for 3 days or after thermal treatment at 150 °C for 2 h, respectively (Fig. 6c and d), showing that the biosynthesized $Zn_xCd_{1-x}S$ QDs are also rather stable in the performance of PL. The high stability in both

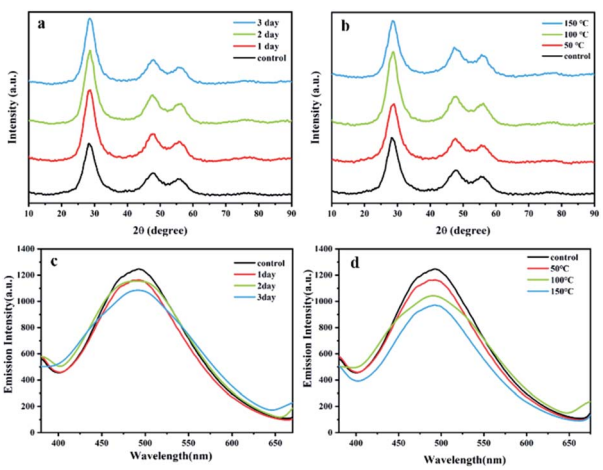

Fig. 6 Gastric acidic or thermal stability of biosynthesized $Zn_xCd_{1-x}S$ QDs. The changes in XRD pattern and PL spectra of biosynthesized $Zn_xCd_{1-x}S$ QDs with molar ratio of Cd^{2+}/Zn^{2+} at 1/30 under simulated gastric acid conditions (pH 1.5 HCl + 0.1 g mL^{-1} pepsin) and different contact times, from 1 day to 3 days ((a) for XRD, (c) for PL), or under heat treatment for 2 h at different temperatures, from 50 °C to 150 °C ((b) for XRD, (d) for PL).

structure and PL activity suggests a great application potential of the $Zn_xCd_{1-x}S$ QDs in the fields of life science and medicine.

To improve the thermal and acidic stability of metal sulfide QDs in both structure and PL activity, an expensive amphiphilic oligomer, PMAO, has been utilized to modify the ZnSe/CdS/ZnS core/shell QD fabricated by wet chemical process. The PL intensity of the QDs-PMAO retained over 85% after treatment in acid solution for 30 min, and the PL intensity dropped to 76% at 90 °C.[31] In contrast, the biosynthesized $Zn_xCd_{1-x}S$ QDs exhibit much higher stability in structure and PL, with 87% PL retention after 3 days of contact in simulated gastric acid and 80% retention at 150 °C for 2 h (Fig. 6). The high stability of the biogenic $Zn_xCd_{1-x}S$ QDs is possibly attributed to the strong electrostatic attraction between Zn^{2+}/Cd^{2+} and the high content of negatively charged acidic amino acids in the EPs, leading to very firm adhesion of EPs to $Zn_xCd_{1-x}S$ QDs to form solid aggregations, which not only enhance the resistance of EPs to pepsin but also boosts the resistance of $Zn_xCd_{1-x}S$ to strong acid and high temperature.

2.4 Biotoxicity test of the biosynthesized $Zn_xCd_{1-x}S$ QDs

High safety and low cytotoxicity are of critical importance for the applications of metal-based QDs in the life science and medical fields, such as biolabeling, biotracing and bioimaging. Morphological and biochemical alteration, loss of cell functionality, chromosome damage and even cell death frequently take place during the uptake of QDs by cells.[2] The cytotoxicity of the SRB-derived $Zn_xCd_{1-x}S$ QDs with different molar ratios of Cd^{2+} to Zn^{2+} under altered concentrations was assessed by using the MC3T3-E1 cell viability test. It was found that at each QD dosage, the viability of cells kept declining with the increase of the molar ratio of Cd^{2+} to Zn^{2+} from 1 : 50 to 1 : 5 due to the highly toxic nature of Cd^{2+}; an evident decrease of the cell viability also occurred when the concentration of the biosynthesized $Zn_xCd_{1-x}S$ QDs increased from 10 to 2000 mg L^{-1} at each molar ratio of Cd^{2+} to Zn^{2+} (Fig. 7a). However, the biogenic $Zn_xCd_{1-x}S$ QDs with the highest Cd^{2+}/Zn^{2+} ratio at 1/5 witnessed a rather high cell viability of 81.6% at 100 mg L^{-1} QD concentration; 51.5% cell viability still occurred even at the highest QD concentration of 2000 mg L^{-1} (Fig. 7a), suggesting that the biosynthesized $Zn_xCd_{1-x}S$ QDs have rather low cytotoxicity. An inhibition zone test also showed that the biosynthesized $Zn_xCd_{1-x}S$ QDs at 100 mg L^{-1} had no effect on the growth of *E. coli* DH5α, whereas the chemosynthetic $Zn_xCd_{1-x}S$ used as a control strongly inhibited cell growth (Fig. 7b), further demonstrating that the biosynthesized $Zn_xCd_{1-x}S$ QDs are much less toxic and highly safe due to the coated EPs on the QD surface.

In the chemical synthesis of metal sulfide QDs, expensive biocompatible organic molecules are widely applied to produce a passivation layer on the surface of QDs in order to reduce their biotoxicity.[33,34] Coating CdS QDs by 3-mercaptopropionic acid resulted in a cell viability of 92% at a low QD concentration of 0.1 mg L^{-1}.[41] CdS conjugates capped by chitosan-based ligands acquired 65% cell viability at a lower concentration of 0.02 mg L^{-1}.[42] The $Zn_xCd_{1-x}S$ QDs with equal molar concentration of Cd and Zn, capped by sodium carboxymethyl cellulose, had a cell viability above 95% at an extremely low concentration of 2.09 × 10^{-3} mg L^{-1}.[33] In contrast, the SRB-derived $Zn_xCd_{1-x}S$ QDs

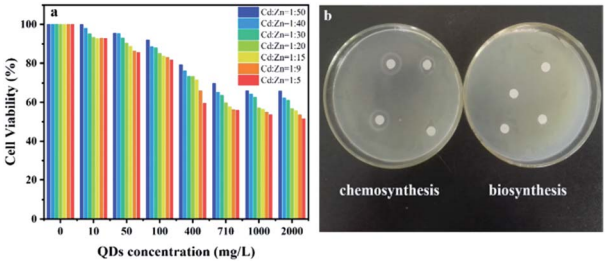

Fig. 7 Biotoxicity test of the biosynthesized $Zn_xCd_{1-x}S$ QDs. Cell viability of MC3T3-E1 after 120 h of contact with the biogenic $Zn_xCd_{1-x}S$ QDs at varied concentrations ranging from 10 to 2000 mg L^{-1}; the initial cell concentration was 3.52 × 10^5 cells per mL, and a sample with no added $Zn_xCd_{1-x}S$ QDs acted as control (a). The inhibition zone assays for chemosynthetic and biosynthetic $Zn_xCd_{1-x}S$ at a concentration of 100 mg L^{-1} using *E. coli* DH5α as model microorganism (b).

gained cell viability of 99.9%–92.7%, 95.4%–85.5% and 91.9%–81.6% at QDs concentrations of 10, 50 and 100 mg L^{-1} when the molar ratio of Cd^{2+} to Zn^{2+} increased from 1 : 50 to 1 : 5, respectively (Fig. 7a). The results demonstrated that the biogenic $Zn_xCd_{1-x}S$ QDs have 2–4 orders of magnitude higher biocompatibility and biosafety than their counterparts produced by chemical routes due to their low Cd content and capping by unique EPs, which endows the biosynthesized ternary $Zn_xCd_{1-x}S$ QDs with a great application potential in medical and biological fields.

2.5 Cell imaging performance of the biosynthesized $Zn_xCd_{1-x}S$ QDs

In vitro HeLa cell imaging was used to test the cell imaging performance of the biosynthesized $Zn_xCd_{1-x}S$ QDs (Fig. 8a–c). Fig. 8a shows that the cells fully kept their integrity in both membrane and morphology after 24 h incubation with the biogenic $Zn_xCd_{1-x}S$ QDs at 10 mg mL^{-1} due to their excellent

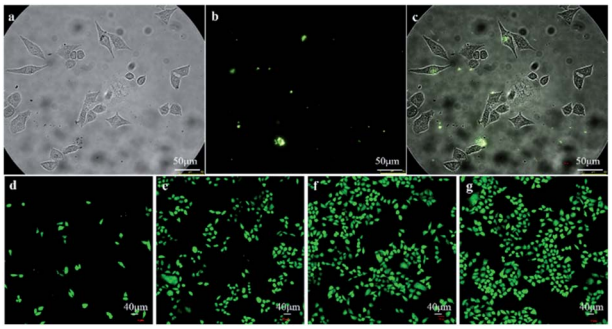

Fig. 8 Cell imaging using the biosynthesized $Zn_xCd_{1-x}S$ QDs. HeLa cells phagocytose the QDs after 24 h of contact ((a) bright field; (b) PL image; (c) overlay image). Growth of cells and membrane integrity over the course of 72 h incubation in the presence of $Zn_xCd_{1-x}S$ QDs ((d) cell population after 24 h contact; (e) population after 48 h contact; (f) population after 72 h contact; (g) population after 72 h culture without QDs as control). The biosynthesized $Zn_xCd_{1-x}S$ QDs have a molar ratio of Cd^{2+} to Zn^{2+} of 1 : 20; the irradiation wavelength was 340–380 nm; the emission wavelength was 550 nm; membrane integrity and cell morphology were evaluated using calcein-AM/PI; the membrane damage is shown by red cell fluorescence; the membrane integrity is shown by green cell fluorescence. In the case of control, the $Zn_xCd_{1-x}S$ QDs were absent.

biocompatibility and high biosafety. Fig. 8b shows that the biosynthesized $Zn_xCd_{1-x}S$ QDs, which reacted with the cells, emitted bright yellow-green PL after 24 h of contact. Fig. 8c demonstrates that the biogenic $Zn_xCd_{1-x}S$ QDs successfully entered the cells and labelled them *via* PL imaging. Further, it was found that the cells kept growing, and the cell membrane integrity was maintained despite a longer contact period of 72 h between the cells and the biogenic $Zn_xCd_{1-x}S$ QDs (Fig. 8d–g), demonstrating that the $Zn_xCd_{1-x}S$ QDs had no effect on the growth of cells concomitant with cell imaging owing to the excellent biocompatibility. The results showed that the biosynthesized $Zn_xCd_{1-x}S$ QDs can be used as a probe for real-time optical cellular imaging as a potential alternative to conventional organic dyes with high toxicity and poor stability.[2–4]

This is the first study to biosynthesize ternary $Zn_xCd_{1-x}S$ QDs using the mixed SRB. The SRB-derived active supernatant, which contains huge amounts of biogenic S^{2-} and high content of peculiar EPs, accounts for the quick extracellular biosynthesis. A very short duration of 30 minutes is required by the active supernatant to give as high as 3.5 g L^{-1} of $Zn_xCd_{1-x}S$ QD productivity, which is comparable to chemical routes. The as-prepared $Zn_xCd_{1-x}S$ QDs have good crystallinity and well-distributed and monodisperse spheres, with ACS of 3.50–4.64 nm, which is independent of the molar ratio of Cd^{2+} to Zn^{2+}. When the molar ratio of Cd^{2+} to Zn^{2+} increases from 1 : 50 to 1 : 5, however, the PL emission wavelength of the biosynthesized $Zn_xCd_{1-x}S$ QDs elevates from 450 nm to 590 nm to obtain multicolor QDs, which almost covers the entire visible region. On the other hand, the biogenic multicolor $Zn_xCd_{1-x}S$ QDs not only have high stability in both chemical structure and PL emission to resist gastric acid and high temperature, but they also have 2–4 orders of magnitude higher biocompatibility and biosafety than the chemically synthesized counterparts. The biogenic $Zn_xCd_{1-x}S$ QDs can enter growing HeLa cells and label them *via* PL imaging, and no toxic effect on cell growth and cell membranes was observed for over 72 h of contact. The high productivity, homogeneous narrow size, PL-tunable multicolor QDs, with great structure and PL stability and extremely excellent biocompatibility and biosafety, endows the SRB-derived $Zn_xCd_{1-x}S$ alloyed QDs with incomparable advantages in biolabeling, biotracing and bioimaging.

Biosynthesis of metal-based nanoparticles or QDs has been universally accepted as environmentally friendly and energy-saving, with less pollution and producing biocompatible products, which is more desirable for application in the life science and medical fields.[1–3] In the contest with chemical routes, however, biosynthesis has long been criticized as having low productivity, being time consuming, with poor control over size, shape and crystallinity, keeping this much-needed technology away from commercial applications.[3,13] The current work entirely breaks through the existing bottlenecks of biosynthesis to drive it from lab to practical application with the help of the mixed SRB. The peculiar EPs secreted by the mixed SRB plays a decisive role in the high yield, tunable PL, stable structure and excellent biocompatibility of the $Zn_xCd_{1-x}S$ QDs. The abnormally high concentration of acidic amino acids (Glu and Asp, 22.8–25.0 mol%) in the peculiar EPs is responsible for the rapid electrostatic absorption of Zn^{2+}/Cd^{2+} for quick nucleation and biosynthesis, while the extremely high content of nonpolar amino acids (Leu, Ala, Ile, Pro, Gly, Val, Phe and Met, 51.7–55.0 mol%) is responsible for controlling the growth of QDs through the formation of tiny cavities *via* hydrophobic bridging and interlinkage.[15] The far tight adhesion between the EPs and the $Zn_xCd_{1-x}S$ QDs due to strong electrostatic reaction accounts for their high stability in the face of gastric acid conditions and high temperature. Particularly, when the molar ratio of Cd^{2+} to Zn^{2+} increased from 1 : 50 to 1 : 5, the amount of EPs adhered into the $Zn_xCd_{1-x}S$ QDs also evidently increased, which not only enhanced the PL redshift from 450 nm to 590 nm at a very low Cd/Zn ratio of 0.02–0.2 but also markedly improved the biocompatibility and biosafety. The multiple functions of the SRB-derived EPs in mediating the biosynthesis of $Zn_xCd_{1-x}S$ QDs are unique, totally different from the most common EPs, such as PC and MT, which are rich in cysteine as a detoxification mechanism.[39,40]

3 Experimental

3.1 Chemicals, microorganisms and media

All chemicals were analytical grade, obtained from Beijing Chemical Industry and used as received without further purification, including lactic acid as an electron donor, Na_2SO_4 (SO_4^{2-}) as an electron acceptor, and $ZnSO_4/CdCl_2$ as precursor Zn^{2+}/Cd^{2+} for the biosynthesis of $Zn_xCd_{1-x}S$ QDs. Deionized water was used to prepare the solutions for both cell culture and biosynthesis of $Zn_xCd_{1-x}S$ QDs.

The mixed SRB, which had performed the highest-ever extracellular biosynthesis of binary metal sulfide QDs,[15] was applied to fabricate the ternary $Zn_xCd_{1-x}S$ alloyed QDs in a modified, easier and faster manner in this work. The media contained 1.0 g L^{-1} NH_4Cl, 0.5 g L^{-1} K_2HPO_4, 0.5 g L^{-1} $MgSO_4$, 0.1 g L^{-1} $CaCl_2$, 0.1 mol L^{-1} lactic acid, and 0.1 mol L^{-1} Na_2SO_4, at pH 7.2.

3.2 Quick biosynthesis of alloyed $Zn_xCd_{1-x}S$ QDs

Fresh media was inoculated with the mixed SRB at a density of 10% (v/v), then the inoculated media was anaerobically incubated at 35 °C. When the mixed SRB reached logarithmic phase after about 4 days of culture, the turbidity of SRB (OD_{600}) increased from 0.1 to 0.6. At that time, the cells were removed by centrifuging at 8000 rpm for 10 min to obtain the supernatant, which contained massive amounts of biogenic H_2S (S^{2-}) from sulfate bioreduction and the peculiar EPs secreted by the mixed SRB.[15] Subsequently, 200 mL of the SRB-derived active supernatant was mixed with 200 mL of mixed $ZnSO_4$ and $CdCl_2$ solutions at different molar ratios (Zn : Cd = 0 : 1, 5 : 1, 9 : 1, 15 : 1, 20 : 1, 30 : 1, 40 : 1, 50 : 1, 1 : 0; total concentration of Zn^{2+} and Cd^{2+} = 0.1 mol L^{-1}). The EPs-mediated precipitation reaction between biogenic S^{2-} and the mixed solution of Zn^{2+} and Cd^{2+} occurred in a 500 mL beaker with a magnetic stirrer (30 rpm, 25 °C). After 30 minutes of contact, the colorless transparent solution gradually changed into a milky-white or slightly milky-yellow suspension liquid, displaying the formation of alloyed $Zn_xCd_{1-x}S$ QDs. Then, the resulting ternary $Zn_xCd_{1-x}S$ QDs were collected by centrifuging (8000 rpm, 10 min), washed three times, respectively, with deionized

water and ethanol. Finally, the $Zn_xCd_{1-x}S$ QDs were freeze-dried under vacuum at −80 °C, ground into a powder and sealed for use.

3.3 Characterization of the extracellular biosynthesized $Zn_xCd_{1-x}S$ QDs

The productivity of ternary $Zn_xCd_{1-x}S$ QDs synthesized using the SRB-derived supernatant and the utilization efficiencies of Zn^{2+} and Cd^{2+} were obtained by calculating the difference of Zn^{2+} and Cd^{2+} concentrations before and after precipitation using inductively coupled plasma optical emission spectrometry (ICP-OES, PerkinElmer Optima 8300, USA). The crystalline phase of the vacuum-dried powder $Zn_xCd_{1-x}S$ alloyed QDs was characterized using X-ray diffraction (XRD, Hitachi Rigaku, Tokyo, Japan) with Cu Kα radiation ($\lambda = 1.5418$ Å). The morphology and size of the $Zn_xCd_{1-x}S$ alloyed QDs were analyzed using transmission electron microscopy (TEM, Hitachi H-800, Tokyo, Japan) at an acceleration voltage of 200 kV with a CCD camera, and further examination was performed using high-resolution transmission electron microscopy (HRTEM). The size distribution and average crystallite size (ACS) of the as-prepared $Zn_xCd_{1-x}S$ QDs were calculated based on the TEM images using the Nano Measurer 1.2 software. For this purpose, 10 pictures and 100 single nanoparticles were randomly chosen. The purity and composition of the ternary QDs were characterized using energy-dispersive X-ray spectroscopy (EDS, Oxford) with an instrument operating at 20 kV. Infrared absorption spectra of the $Zn_xCd_{1-x}S$ QDs were analyzed by Fourier transform infrared spectroscopy (FTIR) using a Thermo Nicolet iS10 spectrophotometer. The thick films of the analytes were prepared by employing a mixture of KBr and the sample. UV-vis absorption and photoluminescence (PL) emission spectra were measured using a Hitachi F-4500 fluorescence spectrometer.

3.4 Amino acid analysis of the mediating proteins coating the $Zn_xCd_{1-x}S$ QDs

The species and concentrations of the amino acids in the mediating proteins attaching to the $Zn_xCd_{1-x}S$ QDs were analysed based on standard procedure (ISO 13903-2005). A certain small amount of the dried powder of $Zn_xCd_{1-x}S$ QDs was added to a 12 mol L^{-1} HCl solution in a hydrolysis flask, followed by adding a few drops of phenol. The hydrolysis flask was sealed after the air was completely displaced with nitrogen. The sealed hydrolysis flask was then placed in a thermotank at 110 °C for 24 h to hydrolyze the proteins. The hydrolysate was then cooled and filtered, and HCL was removed under reduced pressure at 60 °C. Finally, the residual was dissolved in a sodium citrate buffer (pH 2.2) to determine the species and concentrations of amino acids using an amino acid analyser (L-8900, Hitachi high-Technologies Corp., Japan).

3.5 Stability assessment of $Zn_xCd_{1-x}S$ QDs under sterilization and gastric juice

In order to assess the thermal stability of the as-prepared $Zn_xCd_{1-x}S$ QDs after sterilization for applications in medicine and life sciences, variation in PL and XRD images of the resulting product synthesized at Zn/Cd = 30 : 1 was measured; QDs were respectively pre-treated at 50 °C, 100 °C and 150 °C for 2 h in a aqueous solution containing 2.0 g L^{-1} of $Zn_xCd_{1-x}S$ QDs. To assess their stability in a gastric acidic environment, the dried powder of $Zn_xCd_{1-x}S$ QDs at 2.0 g L^{-1} was placed into a simulated stomach juice (a mixed solution of HCl at pH 1.5 and pepsin at 0.1 g mL^{-1}) to contact at 37 °C for 1, 2, and 3 days. The $Zn_xCd_{1-x}S$ QDs were harvested at different contact times to monitor the changes of PL and XRD images. The raw samples without thermal treatment and acidic contact were used as controls.

3.6 Biotoxicity test of the $Zn_xCd_{1-x}S$ QDs produced by the SRB-derived supernatant

3.6.1 MTT assay. All biological tests were carried out according to ISO 10993-5: 2009 (Biological evaluation of medical devices: Tests for *in vitro* cytotoxicity). MTT assay was done using 3-(4,5-dimethylthiazol-2yl)2,5-diphenyltetrazolium bromide; MC3T3-E1 cells were plated (3×10^4 cells per well) in 96-well plates. Cell populations were synchronized in serum-free media for 24 h. Subsequently, the media was suctioned out and replaced with an equal volume of Dulbecco's modified Eagle's medium (DMEM) containing 10% fetal bovine serum (FBS) and incubated for 24 h. The as-prepared $Zn_xCd_{1-x}S$ QD colloidal solutions were added into individual wells at final concentrations of 0.01, 0.05, 0.1, 0.4, 0.71, 1.0 and 2.0 g L^{-1}, respectively. Controls were run with cells and DMEM. After 120 h, all media were aspirated and replaced with 60 L of culture media containing serum in each well. MTT (5 mg mL^{-1}, Sigma-Aldrich, USA) was added into each well and incubated for 4 h in an oven (37 °C, 5% CO_2). Next, 40 μL SDS (Sigma-Aldrich, USA) solution/4% HCl was placed in each well, followed by incubation for 16 h in an oven. Next, 100 μL sample was removed from each well and transferred to a 96-well plate. The absorbance values (Abs) were measured at 595 nm on an iMark™ Microplate Absorbance Reader (Bio-Rad). Percentage cell viability was calculated according to eqn (1). The values of the controls (wells with cells, and no samples) were set to 100% cell viability.

$$\text{Cell vialbility} = \frac{\text{Abs of sample and cells}}{\text{Abs of control}} \times 100\% \quad (1)$$

3.6.2 Inhibition zone test. The model organism *Escherichia coli* (*E. coli*) DH5α was used for the inhibition zone test. The inhibition zone of $Zn_xCd_{1-x}S$ QDs was determined by disk diffusion method in the agar plates. Filter papers impregnated with $Zn_xCd_{1-x}S$ QDs were placed on an *E. coli* DH5α culture dish to monitor the growth inhibition of surrounding cells. The powder $Zn_xCd_{1-x}S$ QDs from $Zn^{2+}/Cd^{2+} = 5 : 1$, the highest ratio of Cd/Zn in this study, was used to test the biological toxicity. Chemically synthesized $Zn_xCd_{1-x}S$ was obtained by precipitating the same mixed solution of Zn^{2+} and Cd^{2+} with 0.1 mol L^{-1} Na_2S instead of the SRB-derived supernatant. Both biogenic and chemically synthesized $Zn_xCd_{1-x}S$ at 0.1 g L^{-1} were compared for their biological toxicity based on the inhibition zone test.

3.7 Application assessment of biosynthesized $Zn_xCd_{1-x}S$ QDs in life science & medicine

3.7.1 Membrane integrity (calcein AM/PI staining). Cell apoptosis was evaluated by calcein AM/PI staining, with AM as the live cell stain (green fluorescence) and PI as dead cell stain

(red fluorescence). HeLa cells were plated (1.5×10^5 cells per well) in 6-well plates. The cell populations were synchronized in serum-free media for 24 h. After that, the media was suctioned and replaced with Dulbecco's modified Eagle's medium (DMEM) containing 10% fetal bovine serum (FBS), then incubated for 24 h. The as-prepared $Zn_xCd_{1-x}S$ QD sample solutions were added to individual wells at final concentrations of 10 mg mL^{-1} for 24 h, 48 h and 72 h, respectively. Controls had cells and DMEM. After co-incubation, the cells in the six-well plates were rinsed with phosphate buffered saline (PBS) to remove excess serum. Then, 2 mM calcein-AM and 2.5 mg mL^{-1} PI were thoroughly mixed with the cells and co-incubated in the dark for 15 min at 37 °C. The cells were then washed and soaked in PBS for 15 min to eliminate nonspecific staining. The cells were observed under a confocal microscope (OLYMPUS, FV10-MPSU).

3.7.2 Cell imaging of the biosynthesized $Zn_xCd_{1-x}S$ QDs. HeLa cells were cultured in high-glucose DMEM media supplemented with 10% FBS and 1% penicillin/streptomycin for 24 h at 37 °C in a humidified 5% CO_2 incubator. Suspensions of the biosynthesized $Zn_xCd_{1-x}S$ alloyed QDs at 10 mg mL^{-1} were prepared from the stock solution with serum-containing DMEM. HeLa cells were seeded in six-well plates with a density of 1.5×10^5 cells per well for the uiptake experiments. The growth medium was replaced with the $Zn_xCd_{1-x}S$ QD suspensions for another 24 h of incubation at 37 °C. The cells were then fixed and recorded with a fluorescence microscope with an emission wavelength at 340–380 nm after the excess $Zn_xCd_{1-x}S$ QDs were removed by washing 3 times with warm PBS.

4 Conclusions

The SRB-derived supernatant is capable of quick and extracellular biosynthesis of the ternary $Zn_xCd_{1-x}S$ QDs. Under mild conditions, as high as 3.5 g L^{-1} of $Zn_xCd_{1-x}S$ QDs with ACS of 3.50–4.64 nm was produced by the active supernatant within 30 minutes, which is comparable to the chemical route. By changing the molar ratio of Cd^{2+} to Zn^{2+}, the PL emission of the $Zn_xCd_{1-x}S$ QDs increases from 450 to 590 nm to yield multicolor QDs. Compared with the chemically synthesized counterparts, the biogenic $Zn_xCd_{1-x}S$ QDs have greater resistance against gastric acid and high temperature as well as 2–4 orders of magnitude higher biocompatibility and biosafety, successfully entering the growing HeLa cells and labelling them *via* PL imaging without detectable harm to cell growth and cell membranes for 72 h. The SRB-secreted peculiar EPs containing abnormally high content of acidic amino acids and extremely high concentration of nonpolar amino acids play a dominant role in the quick and extracellular biosynthesis of $Zn_xCd_{1-x}S$ QDs. The carboxyls in the acidic amino acids offer a large number of negatively charged sites for the absorption of Zn^{2+}/Cd^{2+} for rapid nucleation, while the nonpolar amino acids form small cavities to control the growth of QDs. On the other hand, the electrostatic force-driven firm links between the $Zn_xCd_{1-x}S$ QDs and the peculiar EPs, as well as the increasing amount of EPs adhered to the QDs in smart response to the increasing Cd^{2+} content, account for the high stability in structure and PL emission as well as excellent biocompatibility and biosafety. The multiple functions of the EPs are unique in this biosynthesis.

Conflicts of interest

There are no conflicts to declare. The manuscript was written through contributions of all authors. All authors have given approval to the final version of the manuscript.

Acknowledgements

We highly appreciate and thank financial support from the National Key Research and Development Program (2018YFC1900304, 2018YFC1900301), National Natural Science Foundation of China (21777007), Beijing Natural Science Foundation (8172042), and China Postdoctoral Science Foundation (2020M680364).

Notes and references

1 C. T. Matea, T. Mocan, F. Tabaran, T. Pop, O. Mosteanu, C. Puia, C. Iancu and L. Mocan, *Int. J. Nanomed.*, 2017, **12**, 5421–5431.
2 I. V. Martynenko, A. P. Litvin, F. Purcell-Milton, A. V. Baranov, A. V. Fedorov and Y. K. Gun'ko, *J. Mater. Chem. B*, 2017, **5**, 6701–6727.
3 J. Mal, Y. V. Nancharaiah, E. D. van Hullebusch and P. N. L. Lens, *RSC Adv.*, 2016, **6**, 41477–41495.
4 M. Geszke-Moritz and M. Moritz, *Mater. Sci. Eng., C*, 2013, **33**, 1008–1021.
5 O. V. Singh, *Bio-Nanoparticles–Biosynthesis and Sustainable Biotechnological Implications*, Wiley-Blackwell, John Wiley & Sons, Inc., Hoboken, New Jersey, 2015, p. 33.
6 C. Burda, X. Chen, R. Narayanan and M. A. El-Sayed, *Chem. Rev.*, 2005, **105**, 1025–1102.
7 K. N. Thakkar, S. S. Mhatre and R. Y. Parikh, *Nanomedicine*, 2010, **6**, 257–262.
8 V. Bansal, A. Bharde, R. Ramanathan and S. K. Bhargava, *Adv. Colloid Interface Sci.*, 2012, **179**, 150–168.
9 J. Aguiera-Sigalat, S. Rocton, J. F. Sánchez-Royo, R. E. Galian and J. Pérez-Prieto, *RSC Adv.*, 2012, **2**, 1632–1638.
10 M. R. Hosseini and M. N. Sarvi, *Mater. Sci. Semicond. Process.*, 2015, **40**, 293–301.
11 J. G. Sandana Mala and C. Rose, *J. Biotechnol.*, 2014, **170**, 73–78.
12 T. J. Park, K. G. Lee and S. Y. Lee, *Appl. Microbiol. Biotechnol.*, 2016, **100**, 521–534.
13 M. R. Hosseini, M. Schaffie, M. Pazouki, A. Schippers and M. Ranjbar, *Mater. Sci. Semicond. Process.*, 2013, **16**, 250–255.
14 K. Prasad and A. K. Jha, *J. Colloid Interface Sci.*, 2010, **342**, 68–72.
15 S. Y. Qi, S. H. Yang, J. Chen, T. Q. Niu, Y. F. Yang and B. P. Xin, *ACS Appl. Mater. Interfaces*, 2019, **11**, 10442–10451.
16 C. Gallardo, J. P. Monrás, D. O. Plaza, B. Collao, L. A. Saona, V. Durán-Toro, F. A. Venegas, C. Soto, G. Ulloa,

C. C. Vásquez, D. Bravo and J. M. Pérez-Donoso, *J. Biotechnol.*, 2014, **187**, 108–115.
17 T. J. Park, S. Y. Lee, N. S. Heo and T. S. Seo, *Angew. Chem., Int. Ed.*, 2010, **49**, 7019–7024.
18 Y. Zhang, H. Yang, X. An, Z. Wang, X. Yang, M. Yu, R. Zhang, Z. Sun and Q. Wang, *Small*, 2020, **16**, 2001003.
19 M. Bouroushian, *Electrochemistry of metal chalcogenides*, Springer Science & Business Media, New York, 2010, p. 26.
20 N. G. Imam and M. B. Mohamed, *Superlattices Microstruct.*, 2014, **73**, 203–213.
21 I. Devadoss and S. Muthukumaran, *Phys. E*, 2015, **72**, 111–119.
22 V. P. Kumar, A. Y. Sharma, D. K. Sharma and D. K. Dwivedi, *Optik*, 2014, **125**, 1209–1211.
23 J. Datta, M. Das, A. Dey, S. Halder, S. Sil and P. P. Ray, *Appl. Surf. Sci.*, 2017, **420**, 566–578.
24 M. Yang, Y. Wang, Y. Ren, E. Liu, J. Fan and X. Hu, *J. Alloys Compd.*, 2018, **752**, 260–266.
25 O. Y. Wang, L. Wang, Z. H. Li, Q. L. Xu, Q. L. Lin, H. Z. Wang, Z. L. Du, H. B. Shen and L. S. Li, *Nanoscale*, 2018, **10**, 5650–5657.
26 X. Q. Li, D.-E. Yin, S.-Z. Kang, J. Mu, J. Wang and G. D. Li, *Colloids Surf., A*, 2011, **384**, 749–751.
27 S. Bhandari, R. Begum and A. Chattopadhyay, *RSC Adv.*, 2013, **3**, 2885–2888.
28 H. He, C. Li, Y. Tian, P. Wu and X. Hou, *Anal. Chem.*, 2016, **88**, 5892–5897.
29 N. Yin, L. Liu, P. Li and S. Zhao, *Luminescence*, 2018, **33**, 630–635.
30 V. I. Kochubey, E. K. Volkova and J. G. Konyukhova, *J. Biomed. Opt.*, 2013, **19**, 011020.
31 S. Wang, J. J. Li, Y. Lv, R. Wu, M. Xing, H. Shen, H. Wang, L. S. Li and X. Chen, *Nanoscale Res. Lett.*, 2017, **12**, 380.
32 S. Qu, F. Sun, Z. Qiao, J. Li and L. Shang, *Small*, 2020, **16**, 1907633.
33 A. A. P. Mansur, F. G. De Carvalho, R. L. Mansur, S. M. Carvalho, L. C. De Oliveira and H. S. Mansur, *Int. J. Biol. Macromol.*, 2017, **96**, 675–686.
34 Z. Bujňáková, M. Baláž, E. Dutková, P. Baláž, M. Kello, G. Mojžišová, J. Mojžiš, M. Vilková, J. Imrich and M. Psotka, *J. Colloid Interface Sci.*, 2017, **486**, 97–111.
35 M. A. Osman, A. G. Abd-Elrahim and A. A. Othman, *J. Alloys Compd.*, 2017, **722**, 344–357.
36 L. Jing, S. V. Kershaw, Y. Li, X. Huang, Y. Li, A. L. Rogach and M. Gao, *Chem. Rev.*, 2016, **116**, 10623–10730.
37 M. Liu, Y. He, H. Chen, H. Zhao, W. You, J. Shi, L. Zhang and J. Li, *Int. J. Hydrogen Energy*, 2017, **42**, 20970–20978.
38 L.-J. Tian, W.-W. Li, T.-T. Zhu, G.-H. Zhao, X.-W. Liu, J.-C. Dong, P.-F. An, J.-Y. Ma, F. Shen, C. Qian, B. Hue and H.-Q. Yu, *J. Mater. Chem. A*, 2019, **7**, 18480–18487.
39 E. Grill, E.-L. Winnacker and M. H. Zenk, *FEBS Lett.*, 1986, **197**, 115–120.
40 H. V. Perales-Vela, J. M. Peña-Castro and R. O. Cañizares-Villanueva, *Chemosphere*, 2006, **64**, 1–10.
41 H. Li, M. Li, W. Y. Shih, P. I. Lelkes and W.-H. Shih, *J. Nanosci. Nanotechnol.*, 2011, **11**, 3543–3551.
42 H. S. Mansur, A. A. P. Mansur, A. Soriano-Araujo and Z. I. P. Lobato, *Green Chem.*, 2015, **17**, 1820–1830.